Experimental Analysis of the Joint Statistical Properties of Azimuth Spread, Delay Spread, and Shadow Fading

Albert Algans, Klaus Ingemann Pedersen, *Associate Member, IEEE*, and Preben Elgaard Mogensen, *Member, IEEE*

***Abstract*—Empirical results characterizing the joint statistical properties of the local azimuth spread (AS), the local delay spread (DS), and the shadow (slow) fading component are presented. Measurement data from typical urban, bad urban, and sub urban (SU) environments have been analyzed. It is found that a log-normal distribution accurately fits the distribution function of all the investigated parameters. The spatial autocorrelation function of both AS, DS, and shadow fading can be modeled with an exponential decay function. However, for SU environments the spatial autocorrelation function is better characterized by a composite of two exponential decaying functions. A positive cross correlation is found between the AS and the DS, while both parameters are negatively correlated with shadow fading. All essential parameters required for the implementation of a simulation model considering the joint statistical properties of the AS, DS, and shadow fading are provided.**

***Index Terms*—Channel dispersion, directional channel models, radio propagation.**

I. Introduction

IT IS WELL known from numerous studies that the performance of terrestrial cellular systems is highly dependent on the radio propagation conditions [1], [2]. To give a few examples, the temporal dispersion in the radio channel provides frequency diversity for wideband systems such as wideband code division multiple access (WCDMA), since the degree of frequency selectivity is related to the delay spread (DS) compared to the inverse of the signal bandwidth [3]. Similarly, azimuthal dispersion affects the performance of advanced antenna array systems, as it determines the correlation between spatially separated antennas, and consequently the ability to mitigate fast fading by means of antenna diversity techniques [4]. The azimuthal dispersion also impacts the optimal beamwidth of advanced antenna array systems using the spatial filtering techniques [5]–[7]. Previous studies of azimuthal and temporal dispersion have mainly focused on the shape of the local power azimuth spectrum (PAS) and the local power delay spectrum (PDS) averaged over a few tens of wavelengths. These spectra have been analyzed by means of either simple geometrical models [8]–[10], ray tracing studies [11], or analysis of measurement data [12], [13]. Shadow fading is another propagation mechanism, which impacts the performance of wireless systems. Earlier studies of shadow fading have mainly focused on identifying an appropriate distribution function which accurately describes this mechanism [14], [15], as well as the spatial autocorrelation properties [16]–[19]. However, the global joint statistical properties of the local DS, the local azimuth spread (AS), and shadow fading in macro cellular outdoor environments still remain to be characterized. This includes describing the distribution function of the local AS and the local DS, how the local AS and DS vary as the mobile station (MS) moves along a certain route (i.e., autocorrelation properties), mutual dependency between the AS, DS, and shadow fading (i.e., cross-correlation properties), etc. Such a description is important for the implementation of realistic network level simulators of modern wideband mobile communication systems applying advanced antenna array systems such as the Universal Mobile Telecommunications System (UMTS).

Functions that characterize the joint random behavior of AS, DS, and shadow fading are, therefore, extracted from experimental data collected during extensive measurement campaigns. The three parameters of interest are extracted from measurements conducted with a stand-alone testbed equipped with an antenna array at the base station (BS). All the considered measurement scenarios are characterized as outdoor macro cellular cases, with the BS antenna array elevated above any local scatterers.

The paper is organized as follows. In Section II, the measurement system and the investigated environments are described. The applied signal model and method for analyzing the collected measurement data are outlined in Section III. Sections IV–VI present the results from an extensive analysis of the measurements, including simple models of the pdf of the parameters under study, the spatial autocorrelation function, and cross-correlation properties. Based on the empirical results, a simple model for simulation of the three random variables describing the local AS, the local DS, and shadow fading component is outlined in Section VII. Finally, some concluding remarks are given in Section VIII.

II. Measurement Campaign

A. Stand-Alone Testbed

The measurement campaign was conducted using the wideband stand-alone testbed developed within the project, ACTS, Technology in Smart Antennas for UNiversal Advanced Mobile

Manuscript received March 20, 2001; revised September 14, 2001.

A. Algans is with the Center for Personkommunication (CPK), Aalborg University, Aalborg 9220, Denmark (e-mail: aalgans@cpk.auc.dk).

K. I. Pedersen is with the Nokia Networks, Aalborg 9220, Denmark (e-mail: Klaus.I.Pedersen@nokia.com).

P. E. Mogensen is with the Center for Personkommunication (CPK), Aalborg University, Aalborg 9220, Denmark and also with the Nokia Networks, Aalborg 9220, Denmark (e-mail: Preben.Mogensen@nokia.com).

Publisher Item Identifier S 0733-8716(02)03294-8.

TABLE I
SUMMARY OF MACRO CELLULAR MEASUREMENT ENVIRONMENTS

Class	BS Antenna Height	Description of environment
TU	20 m and 32 m	The city of Aarhus, Denmark. Uniform density of buildings ranging from 4-6 floors. Irregular street layout. Measurements carried out along six different routes with an average length of 2 km. No line-of-sight between MS and BS. MS-BS distance varies from 0.2 km to 1.1 km.
TU	21 m	Stockholm city, Sweden (Area #1). Heavily built up area with a uniform density of buildings, ranging from 4-6 floors. Ground is slightly rolling. No line-of-sight between MS and BS. MS-BS distance varies from 0.2 km to 1.1 km.
BU	21 m	Stockholm city, Sweden (Area #2). Mixture of open flat areas (river) and densely build up zones. Ground is slightly rolling. No line-of-sight between MS and BS. MS-BS distance varies from 0.9 km to 1.6 km.
SU	12 m	The city of Gistrup, Denmark. Medium-sized village with family houses of one-two floors and small gardens with trees and bushes. Typical Danish residential area. The terrain around the village is rolling with some minor hills. No line-of-sight between MS and BS. MS-BS distance varies from 0.3 km to 2.0 km.

Infrastructure, Part II (TSUNAMI II) [20]. The setup consists of a BS equipped with an eight-element uniform linear antenna array and a MS with an omni directional dipole antenna. The MS is equipped with a differential global positioning system (GPS) and an accurate position encoder so its location is accurately known by combining the information from these two devices. MS displacements of less than one centimeter can, therefore, be detected. The system is designed for uplink transmission, i.e., from the MS to the BS. Simultaneous channel sounding is performed on all eight branches, which makes it possible to estimate the azimuth of the impinging waves at the BS. The sounding signal is a maximum length linear shift register sequence of the length 127 chips, clocked at a chip-rate of 4.096 Mcps. The testbed operates at a carrier frequency of 1.8 GHz. Additional information regarding the stand-alone testbed can be found in [12] and [21].

B. Investigated Environments

A variety of measurement campaigns has been conducted in different environments, with the emphasis on macro cellular scenarios. In this context, macro cellular refers to a scenario where the BS antenna array is elevated above rooftop level of the surrounding buildings. More than 13 Gbyte of measurement data have been collected along routes in different environment classes. The investigated environments are classified as; typical urban (TU), bad urban (BU), and sub urban (SU). This classification is made according to the definitions in COST 207 [22]. Hence, the temporal dispersion observed in the TU environments is similar to the temporal dispersion of the COST 207 TU model. A summary of the different measurement campaigns is presented in Table I. Notice that measurements in Aarhus are conducted at two different BS antenna heights in order to investigate how this impacts on the propagation characteristics under consideration in this study.

In the sequel, we will use TU-32 and TU-20 when we refer to the TU measurements in Aarhus with the BS antenna elevated 32 m and 20 m above ground level. Similarly, TU-21 refers to the TU measurements in Stockholm with the BS antenna positioned 21 m above ground level.

III. ANALYSIS OF MEASUREMENT DATA

A. Signal Model

Extending Bello's terminology [23], we can define the radio channels azimuth-delay spread function at the BS according to

$$h(\phi,\tau)=\sum_{l=1}^{L}\alpha_l\delta(\phi-\phi_l,\tau-\tau_l) \tag{1}$$

where the parameters α_l, τ_l, and ϕ_l are the complex amplitude, delay, and incidence azimuth of the lth impinging wave at the BS. In general, $h(\phi,\tau)$ is considered to be a time-variant function, since the constellation of the impinging waves is likely to change as the MS moves along a certain route. However, this dependency is omitted in writing (1) in order to simplify the notation. Based on (1), let us define the local average power azimuth-delay spectrum as

$$P(\phi,\tau)=E\left\{\sum_{l=1}^{L}|\alpha_l|^2\delta(\phi-\phi_l,\tau-\tau_l)\right\} \tag{2}$$

where $|\cdot|$ takes the absolute value of the argument and $E\{\cdot\}$ denotes expectation. The PAS and the PDS can subsequently be expressed as

$$P_A(\phi) = \int P(\phi,\tau)d\tau \tag{3}$$

$$P_D(\tau) = \int P(\phi,\tau)d\phi. \tag{4}$$

From these functions we can define the radio channels local AS σ_A and the local DS σ_D as the root second central moment of $P_A(\phi)$ and $P_D(\tau)$, respectively. The values of the local AS and DS are likely to vary as the MS moves within a certain environment. Hence, we can characterize σ_A and σ_D as being random variables, with the joint pdf $f(\sigma_A,\sigma_D)$. Their marginal pdfs are

$$f_A(\sigma_A) = \int f(\sigma_A,\sigma_D)d\sigma_D \tag{5}$$

$$f_D(\sigma_D) = \int f(\sigma_A,\sigma_D)d\sigma_A. \tag{6}$$

Notice here that the function $f(\sigma_A,\sigma_D)$ can be interpreted as the global joint pdf of the local AS and DS. Assuming that the expectation in (2) is computed over the radio channel's fast fading component, we can, furthermore, apply the approximation

$$\iint P(\phi,\tau)d\phi d\tau = h_{\text{channel}} \cong h_{\text{loss}}(d)h_s \tag{7}$$

where h_{channel} is the radio channel's integral path loss, $h_{\text{loss}}(d)$ is the deterministic long term distance dependent path loss, while h_s is the channel's shadow fading component, which is typically being modeled with a log-normal distributed random variable [14], [15]. The global pdf of h_s is denoted $f_s(h_s)$. The global degree of shadow fading is described by the root second central moment of the random shadow fading component expressed in decibel, i.e.,

$$\sigma_s = \text{Std}\{10\log_{10}(h_s)\}, \tag{8}$$

where $\text{Std}\{\ \}$ denotes standard deviation.

B. Estimation of Radio Channel Parameters

The parameters of each impinging wave in (1) are estimated from measurement data using the space alternating generalized expectation maximization (SAGE) algorithm [24]. This scheme provides a computationally efficient method for calculating the maximum-likelihood estimate of the wave parameters from the collected measurement data. Application of the SAGE algorithm for channel estimation is outlined in [25] and [26]. The SAGE algorithm requires detailed knowledge of the response of the measurement system in order to return reliable and accurate estimates. For this purpose, the complex radiation pattern of each BS antenna array element has been measured in an anechoic chamber. The impulse response of the measurement system has also been measured by connecting the transmitter and the receiver with a cable. Both the measured radiation pattern and the impulse response have been included in the SAGE algorithm.

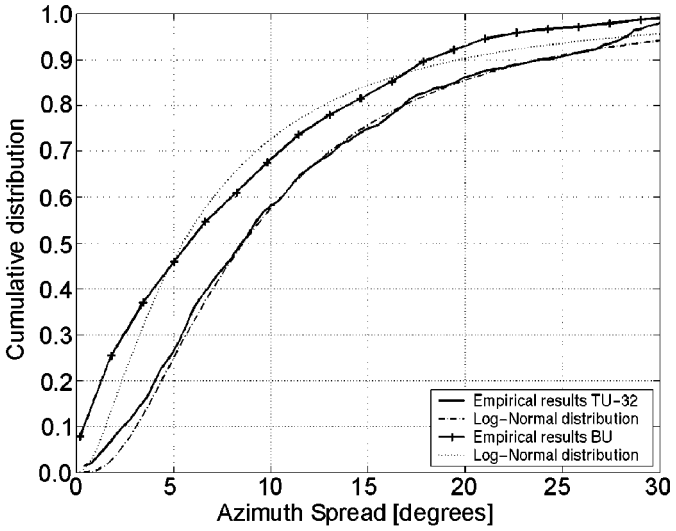

Fig. 1. Examples of empirical cumulative distribution function (cdf) of AS obtained in different environments. The cdf of a log-normal distribution is fitted to the empirical results for comparison.

The radio channels' azimuth-delay spread function (1) is estimated for every 0.4 wavelength segment of the measurement route using the SAGE algorithm. Subsequently, an estimate of the local average power azimuth-delay spectrum is obtained by computing the expectation in (2) over a distance of 30 wavelengths, corresponding to approximately 5 m at the operating carrier frequency. This distance is considered to be sufficiently large, in order to average over the fast fading component of the radio channel. Based on estimates of $P(\phi,\tau)$ for every 5 m segment of the different measurements, we obtain sample estimates of the local AS, DS, and h_{channel}. As the distance between the BS and MS is known for every 5 m segment, the shadow fading component h_s can be decomposed from h_{channel} for each measurement segment. The procedure for this operation is discussed in details later in Section IV-C.

IV. PDF OF THE AS, DS, AND SHADOW FADING

A. PDF of the AS

Based on a large sample set of the estimated local AS in the different environments, it is possible to plot the empirical AS distribution for each environment class. Fig. 1 shows the empirical cdf of the AS for the TU-32 and the BU environment. The relative low values of AS indicate that the incoming field at the BS antenna array is highly concentrated in azimuth. Although not shown here, the shape of the local PAS is found to follow a Laplacian function for most cases (see [12] for more information on the local PAS). The cdf of two log-normal distributions is fitted to the empirical results and plotted for comparison in Fig. 1. It is observed that the log-normal distribution provides an accurate match for the results obtained in both TU-32 and BU. For comparison, other distributions such as e.g., a Rayleigh cdf have also been fitted to the empirical results. However, the log-normal distribution seems to provide the best match for all the considered cases. Hence, it has also been found that the log-normal distribution fits the empirical cdf of the AS

TABLE II
SUMMARY OF THE FIRST AND SECOND CENTRAL MOMENTS OF THE AS, DS, AND SHADOW FADING IN THE DIFFERENT ENVIRONMENTS

Class	σ_s	$E\{\sigma_A\}$	μ_A	ε_A	$E\{\sigma_D\}$	μ_D	ε_D
TU-32	7.3 dB	8^0	0.74	0.47	0.8 μs	-6.20	0.31
TU-21	8.5 dB	8^0	0.77	0.37	0.9 μs	-6.13	0.28
TU-20	7.9 dB	13^0	0.95	0.44	1.2 μs	-6.08	0.35
BU	10.0 dB	7^0	0.54	0.60	1.7 μs	-5.99	0.46
SU	6.1 dB	8^0	0.84	0.31	0.5 μs	-6.40	0.22

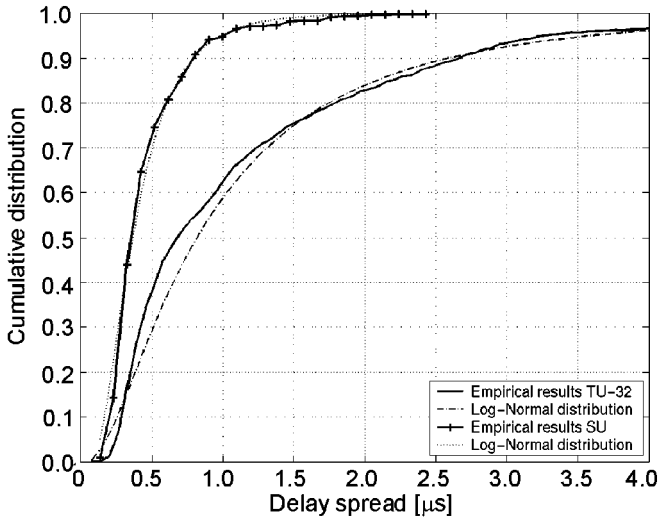

Fig. 2. Examples of empirical cdfs of the DS obtained in different environments. The cdf of a log-normal distribution is fitted to the empirical results for comparison.

obtained from the SU environment, TU-21 and TU-20. We will, therefore, approximate $f_A(\sigma_A)$ with a log-normal pdf.

This implies that the random variable describing the local AS can be expressed as

$$\sigma_A = 10^{\varepsilon_A X + \mu_A} \tag{9}$$

where X is a zero-mean Gaussian distributed random variable with unit variance, $\mu_A = E\{\log_{10}(\sigma_A)\}$ is the global logarithmic mean of the local AS, and $\varepsilon_A = \mathrm{Std}\{\log_{10}(\sigma_A)\}$ is the logarithmic standard deviation of the AS. From the measurements in Aarhus it has been observed that the AS decreases from approximately 13° (TU-20) to 8° (TU-32) when the BS antenna position is reduced by 12 m. Similar results were presented in [12] and [27]. However, no dependency between μ_A and the distance between the MS and BS has been found, although ray-tracing results presented in [11] show a systematic relation between MS-BS distance and the AS. More results concerning the AS in the different environments are summarized in Table II.

B. PDF of DS

Fig. 2 shows the empirical cdf of the DS in the TU-20 and the SU environment. It is observed that the DS is significantly higher in the TU-20 environment compared to the SU environment. However, in both cases the shape of the local PDS seems to follow an exponential decay. The higher DS in TU-20 is to be expected, since TU environments are typically characterized as rich scattering areas leading to a higher dispersion relative to SU environments. Inherently, this is part of the classification of the two propagation environments. For comparison, the cdf of a log-normal distribution is fitted to the empirical results and plotted into Fig. 2. Based on these results, it seems to be a good approximation to model the local distribution of the DS with a log-normal distributed variable, i.e.,

$$\sigma_D = 10^{\varepsilon_D Y + \mu_D}, \tag{10}$$

where Y is a zero-mean Gaussian distributed random variable with unit variance, $\mu_D = E\{\log_{10}(\sigma_D)\}$ is the global logarithmic mean of the local DS, and $\varepsilon_D = \mathrm{Std}\{\log_{10}(\sigma_D)\}$ is the logarithmic standard deviation of the DS. The analysis of the measurements collected in the BU environment confirms that the model in (10) is also accurate for this environment. From the TU measurements in Aarhus, it has furthermore been observed that the average DS decreases with increasing the BS antenna height from approximately 1.2 to 0.8 μs (see Table II).

C. PDF of Shadow Fading

The shadow fading component is extracted from the measurement data under the assumption that the deterministic distance path loss can be expressed in decibel as

$$10\log_{10}\left(h_{\mathrm{loss}}(d)\right) = A + B\log_{10}(d) \tag{11}$$

where d is the distance between the BS and MS expressed in km. As an example, the Okumura-Hata model [28] is based on a similar structure. Substituting (11) into (7), the following relationship is obtained:

$$10\log_{10}\left(h_{\mathrm{channel}}(d)\right) = A + B\log_{10}(d) + 10\log_{10}(h_s). \tag{12}$$

For each 5 meter section, we know the variable set $\{10\log_{10}(h_{\mathrm{channel}}(d_i)); d_i\}$, where d_i is the distance to the BS and $h_{\mathrm{channel}}(d_i)$ is the measurement of the integral path loss from the ith measurement segment, respectively. Assuming that $E\{10\log_{10}(h_s)\} = 0.0$ dB, the parameters A and B can be obtained as the least square estimate from a large number of measurements. Subsequently, the shadow fading component can be isolated from each measurement segment by rearranging (12). As an example, a scatter plot of the pair $\{10\log_{10}(h_{\mathrm{channel}}(d_i)); d_i\}$ is pictured in Fig. 3 based on measurements obtained in TU-32. The linear regression line fitting the data is also plotted. The shadow fading component is thus the distance between the points and the linear regression line.

It is found that a log-normal distribution function provides a good match to the empirical pdf of the shadow fading component. This observation is in coherence with numerous other studies, see [1], [13], and [14] among others. The shadow fading standard deviation is found to be in the range $\sigma_s = [6\text{–}10]$ dB depending on the environment class, with the largest standard deviation observed in the BU and the smallest in SU environments. These findings are in accordance with previous findings

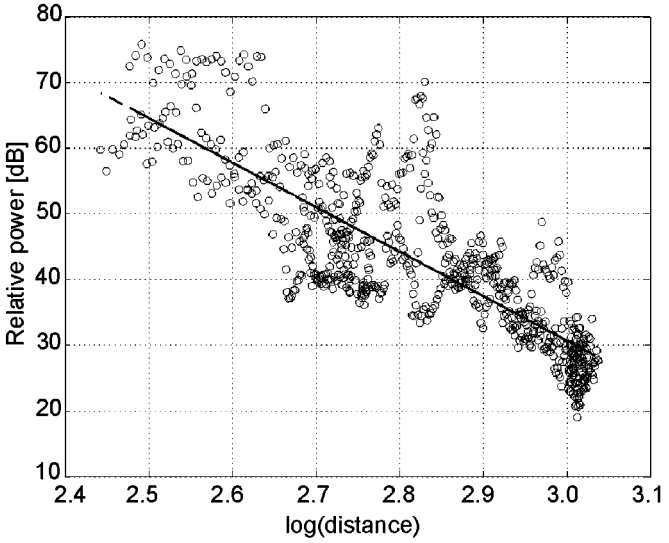

Fig. 3. Scatter plot of the relative received power versus distance in the TU-32 environment.

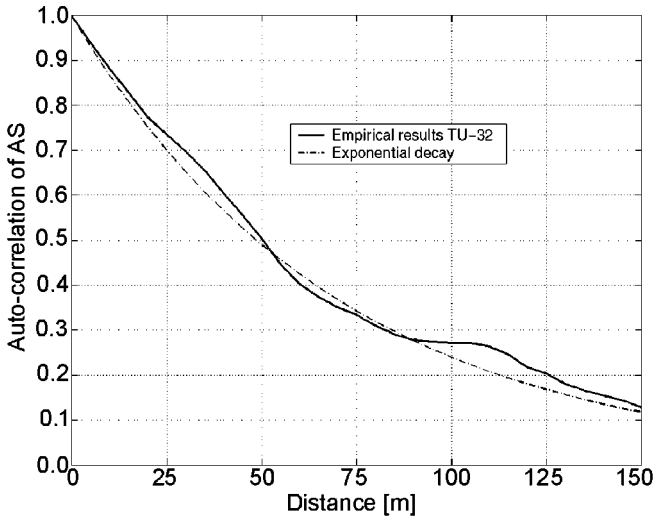

Fig. 4. Empirical spatial autocorrelation function of AS in TU-32. An exponential decaying function is matched to the empirical results with $d_A = 70$ m.

in the open literature as well. Hence, the random variable describing the shadow fading component can be expressed as

$$h_s = 10^{\sigma_s Z/10} \tag{13}$$

where Z is a zero-mean Gaussian random variable with unit variance.

D. Summary of First- and Second-Order Central Moments

Table II contains a summary of the first and second-order central moments of the AS, DS, and shadow fading component for the different environment classes. The moments of the logarithmic AS and DS are also presented, as these are required in order to model the random variables describing the DS and AS according to (9) and (10). From the measurements in Aarhus (TU-32 and TU-20) it is observed that both DS and AS varies with the BS antenna position, while the standard deviation of shadow fading remains approximately the same for the two antenna heights.

V. Spatial Auto-correlation Function of the AS, DS, and Shadow Fading

A. Spatial Autocorrelation Function of the AS

The spatial autocorrelation function of the AS, is a measure of how fast the local AS evolves as the MS moves along a certain route. An example of the empirical spatial autocorrelation function of the AS in the TU-32 environment is pictured in Fig. 4. For comparison, an exponential decay is matched to the empirical results. It is observed that the exponential decaying function accurately models the spatial autocorrelation function of the AS, i.e.,

$$\rho_A(d) = \exp\left(-\frac{d}{d_A}\right) \tag{14}$$

where d is the distance traveled by the MS and d_A is the decorrelation distance of the AS. A short decorrelation distance indicates that the AS experienced at the BS changes quickly as the MS moves, while a longer decorrelation distance corresponds to an environment with a higher degree of stationarity. The function in (14) is also found to provide a good model of the spatial autocorrelation function of the AS in BU environments.

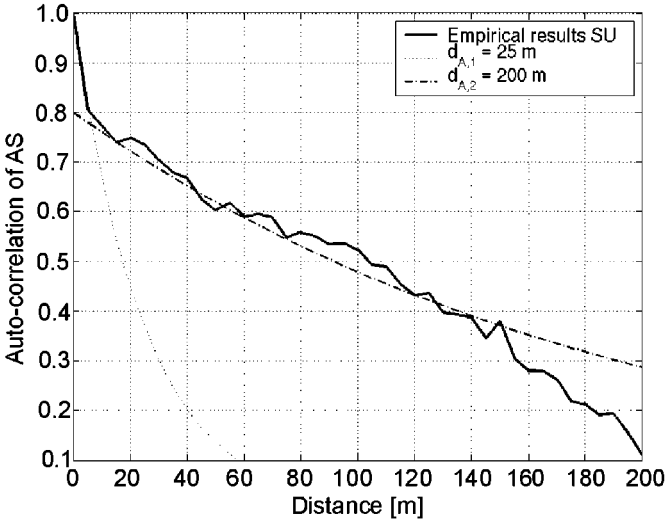

Fig. 5. Empirical spatial autocorrelation function of AS in SU. A double exponential decaying function is matched to the empirical results.

However, in SU environments the model in (14) seems to be less accurate. An example of the empirical spatial autocorrelation function obtained from the SU environment is plotted in Fig. 5. For this type of environment, a double exponential model seems to better model the autocorrelation function, so

$$\rho_A(d) = k\exp\left(-\frac{d}{d_{A,1}}\right) + (1-k)\exp\left(-\frac{d}{d_{A,2}}\right) \tag{15}$$

where $d_{A,1}$ and $d_{A,2}$ are the short and long decorrelation distances of the two components. The parameter $k \in [0,1]$ expresses the mutual strength between the short and the long decorrelation component. The function in (15) is plotted in

TABLE III
SPATIAL DECORRELATION DISTANCE FOR AS, DS, AND SHADOW FADING IN DIFFERENT ENVIRONMENTS EXPRESSED IN METERS. THE TWO NUMBERS PRESENTED FOR SU, CORRESPONDING TO THE SHORT AND LONG DECORRELATION COEFFICIENTS

Class	d_A	d_D	d_s
TU-32	50	40	45
TU-21	50	50	25
TU-20	75	50	55
BU	65	95	120
SU	25/200 (k=0.2)	15/150 (k=0.3)	30/200 (k=0.4)

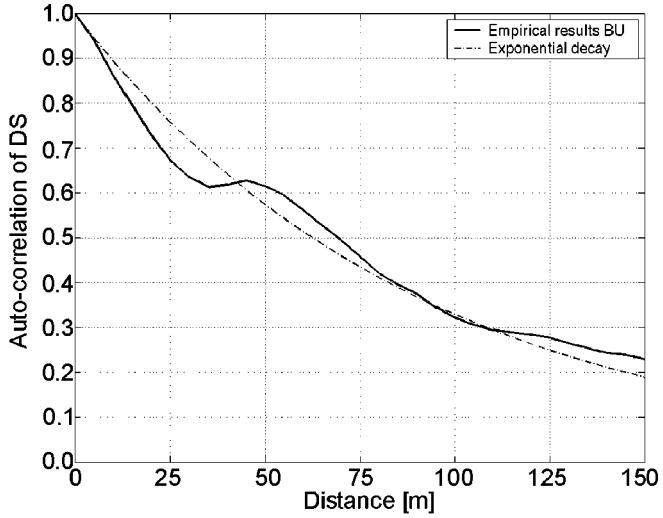

Fig. 6. Empirical spatial autocorrelation function of the DS obtained in BU environments. An exponential decaying function is fitted to the empirical results.

Fig. 5 with $d_{A,1} = 25$ m, $d_{A,2} = 200$ m, and $k = 0.2$. For this particular case $d_{A,1} = 25$ m corresponds approximately to the average size of the houses in the SU environment, while $d_{A,2} = 200$ m is on the order of the average distance between street crossings. Hence, the parameters in (15) can be related to the physical topology of the environment. The decorrelation distances for all the considered environments are summarized in Table III.

B. Spatial Autocorrelation Function of DS

An example of the spatial autocorrelation function of the DS obtained from the BU environment is presented in Fig. 6. An exponential decaying function is plotted for comparison, which accurately matches the empirical results. Hence, the autocorrelation function of the DS in BU environments can be modeled according to

$$\rho_D(d) = \exp\left(-\frac{d}{d_D}\right) \tag{16}$$

where d_D is the decorrelation distance of the DS. A short decorrelation distance indicates that the DS changes quickly as the MS moves. Thus, d_D and the MS speed give an idea of how fast the radio channels coherence bandwidth changes [1] and, therefore, e.g., also how often RAKE finger allocation and a search should be conducted [6], etc. The model in (16) is also found to be valid for TU environments, while the model

$$\rho_D(d) = k\exp\left(-\frac{d}{d_{D,1}}\right) + (1-k)\exp\left(-\frac{d}{d_{D,2}}\right) \tag{17}$$

provides a better match for SU environments. Here $d_{D,1}$ and $d_{D,2}$ is the short and long decorrelation distance of the two components, while $k \in [0,1]$ expresses the weighting between the two components.

C. Spatial Autocorrelation Function of Shadow Fading

The spatial autocorrelation of shadow fading has been investigated in numerous studies, and therefore only shortly discussed here. In accordance with Gudmundson [16] and Mawira [17], we have found that a single exponential decay accurately matches the empirical spatial autocorrelation function obtained from TU and BU environments, with decorrelation distance d_s. However, for the SU environment a double exponential decay seems to provide a better match to the empirical autocorrelation function. This finding is in coherence with Sørensen's results reported in [19].

D. Summary of Decorrelation Distances

Table III contains a summary of the mean decorrelation distances of the AS, DS, and shadow fading for the different environments expressed in meters. Notice that for the SU environment, two decorrelation distances are reported. These correspond to the short and the long decorrelation distance, since the spatial autocorrelation function is characterized by these two parameters in SU environments, see (15) and (17). The parameter k is also reported for the SU environment, to indicate the weight factor between the short and long component. It is worth noticing from Table III that the decorrelation distance is almost identical for both the AS, DS, and shadow fading in each of the three environment classes. Secondly, the spatial autocorrelation function has the same shape for all three parameters. From the measurements in Aarhus it is furthermore observed that the decorrelation distance increases by approximately 25%–50% when the BS antenna is located at the lowest position. These observations indicate that the radio propagation mechanisms leading to the AS, DS, and shadow fading are related.

VI. CROSS-CORRELATION PROPERTIES

A. Motivation for Analysis

In order to be able to jointly simulate the random behavior of the AS, DS, and shadow fading it is not sufficient to have knowledge of the pdf and the spatial autocorrelation function of the three variables. Information on the cross correlation between the variables is also needed. As all three variables are found to be log-normal distributed as observed in Section IV, the most convenient method for simulating them on a computer would probably be to generate zero-mean independent Gaussian random variables with unit variance. Subsequently, these Gaussian variables can be mapped to the AS, DS, and

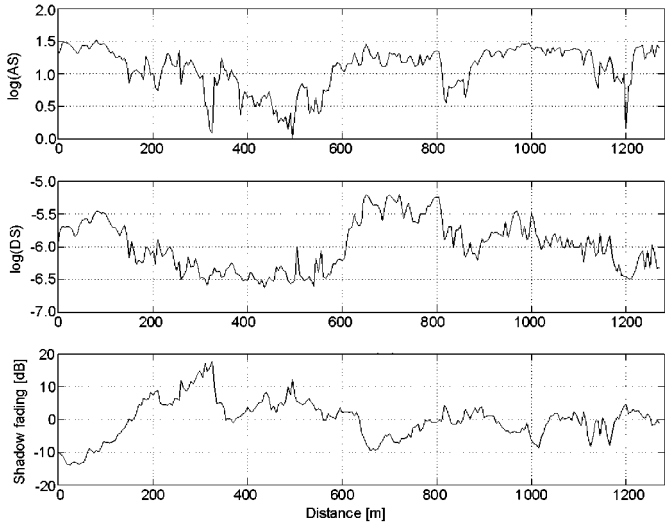

Fig. 7. Example of evolution of $\log(\mathrm{AS})$, $\log(\mathrm{DS})$, and shadow fading along a route in the TU-20 environment.

shadow fading according to (9), (10), and (13). However, this method would result in random variables with zero-cross correlation. To generate correlated variables, we could perform a linear transformation, to obtain a new set of correlated Gaussian processes (X, Y, and Z). Afterwards, these can be mapped to the AS, DS, and shadow fading according to (9), (10), and (13). In order to be able to conduct this operation we need knowledge of the cross correlation between the logarithmic AS (X), the logarithmic DS (Y), and shadow fading expressed in decibel (Z). This information is needed in order to determine the coefficients of the aforementioned linear transformation. We will, therefore, quantify the cross-correlation coefficient between the three considered variables in the logarithmic domain in the following. The cross-correlation coefficient between a and b is computed according to

$$\rho\langle a,b\rangle = \frac{\sum_{i=1}^{N}\left(a(i)-\bar{a}\right)\left(b(i)-\bar{b}\right)}{\sqrt{\sum_{i=1}^{N}\left(a(i)-\bar{a}\right)^2\sum_{i'=1}^{N}\left(b(i')-\bar{b}\right)^2}} \tag{18}$$

where $\bar{a}$ and $\bar{b}$ are the sample means of the sets $\{a(i)\}$ and $\{b(i)\}$ with set size N, respectively.

As an example, Fig. 7 pictures the evolution of the logarithmic AS and DS, and the shadow fading component expressed in decibel along a measurement route in the TU-32 environment. Based on a visual inspection, there seems to be some correlation between the three variables. The AS and DS tend to increase and decrease at the same positions, while the shadow fading component typically is in a fade when the AS and DS are relatively high. A summary of the cross-correlation coefficients is presented later in Section VI-E for all the considered environments.

B. Cross Correlation Between AS and DS

A scatter plot with pairs of $\log(\mathrm{AS})$ and $\log(\mathrm{DS})$ is shown in Fig. 8. The linear regression line fitted to the presented data

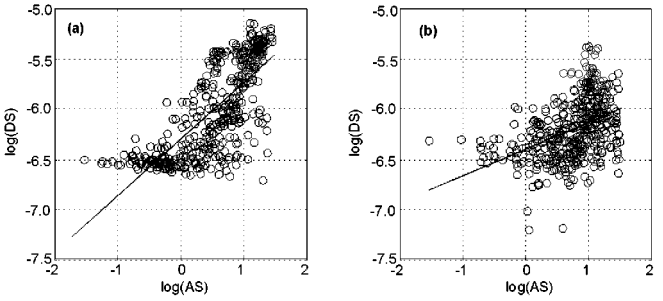

Fig. 8. Scatter plot of log(AS) and log(DS). (a) BU environments. (b) TU-32 environments.

TABLE IV
EMPIRICAL CROSS–CORRELATION COEFFICIENTS FOR THE DIFFERENT ENVIRONMENT CLASSES. BOTH FOR THE AS, DS, AND SHADOW FADING EXPRESSED IN LINEAR AND LOGARITHMIC

Class	$\rho\langle\sigma_A,\sigma_D\rangle$	$\rho\langle\sigma_A,\sigma_D\rangle$ log	$\rho\langle\sigma_A,h_s\rangle$	$\rho\langle\sigma_A,h_s\rangle$ log	$\rho\langle\sigma_D,h_s\rangle$	$\rho\langle\sigma_D,h_s\rangle$ log
TU-32	0.39	0.44	-0.51	-0.7	-0.38	-0.4
TU-21	0.34	0.36	-0.47	-0.54	-0.34	-0.5
TU-20	0.6	0.6	-0.65	-0.72	-0.44	-0.48
BU	0.69	0.67	-0.44	-0.53	-0.55	-0.69
SU	0.46	0.46	-0.47	-0.5	-0.38	-0.46

is also plotted. It is observed that there is a positive cross correlation, indicating that the mechanisms leading to azimuthal dispersion and temporal dispersion are related. A stronger correlation is observed for the BU environment compared to the TU-32 environment. Furthermore, these results indicate that the potential space and frequency diversity gains are highly correlated, since a low DS results in a high coherence bandwidth and a low AS results in a stronger correlation between signals received by two spatially separated antennas. From Table IV, it is furthermore observed that the cross-correlation coefficient between AS and DS increases as the BS antenna position is reduced (TU-32 to TU-20).

C. Cross Correlation Between AS and Shadow Fading

On average, a negative cross correlation between the shadow fading and the AS is observed from Fig. 9. However, if the measurement data are filtered, so we mainly consider the MS positions in the vicinity of street crossings, then we observe a positive cross correlation. Hence, it seems that two competing mechanisms are leading to a positive and a negative cross correlation, respectively. This can be justified intuitively as follows. When the MS is in a street canyon the signal is likely to propagate from the MS to the BS via a few rooftop diffractions close to the MS, leading to a relative low AS. On the other hand, once the MS is located in a street crossing, there is a higher likelihood of having more distant dominant scatterers creating a higher AS, assuming there is no line-of-sight. Provided that a smaller fraction of the signal from the MS reaches the BS, when positioned in a street crossing compared to a street canyon, then we have the aforementioned cross-correlation properties. Therefore, the number of street crossings along a measurement route

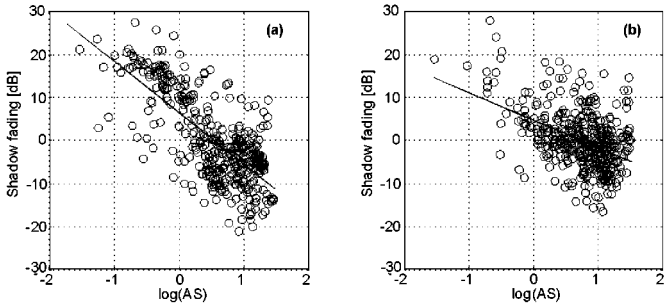

Fig. 9. Scatter plot of shadow fading and log(AS). (a) BU environments. (b) TU-32 environments.

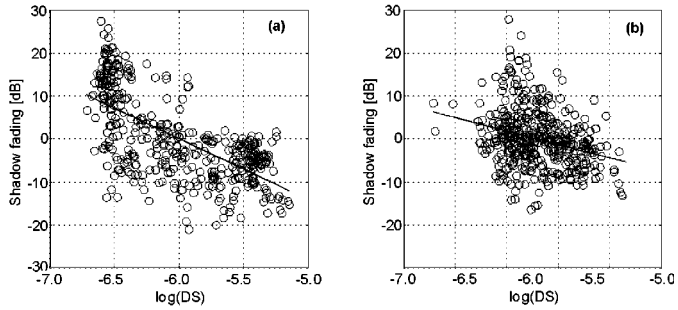

Fig. 10. Scatter plot of shadow fading and log(DS). (a) BU environments. (b) TU-32 environments.

tends to impact on the cross-correlation coefficient between AS and shadow fading.

D. Cross Correlation Between Shadow Fading and DS

A negative cross correlation is also observed between shadow fading and the DS as shown in Fig. 10. This experimental finding matches Greensteins theoretical predictions reported in [29]. This behavior can be explained as follows. Assuming that the PDS $P_D(\tau)$ can be described with a decreasing function (say exponential decay), so the paths with the shortest delay carry the most power. During a deep shadow fade it is therefore likely that paths with the shortest delay exhibit a deep fade as well, leading to a more uniform (rectangular) shape of the PDS, which results in higher DS. Thus, leading to a negative cross correlation between shadow fading and the DS.

E. Summary of Cross-Correlation Coefficients

Table IV presents a summary of the cross-correlation coefficients for the different environment classes. The cross-correlation coefficients are presented for both the AS, DS, and shadow fading expressed in a linear scale and logarithmic domain. From Table IV we can conclude that the scattering mechanisms that create the AS and the DS are strongly related in BU environments since the cross correlation is 0.75 (logarithmic domain). In the TU and SU environments there seems to be a lower cross correlation. The cross-correlation coefficient between AS and shadow fading, and DS and shadow fading is considered to be moderate in all the investigated environments.

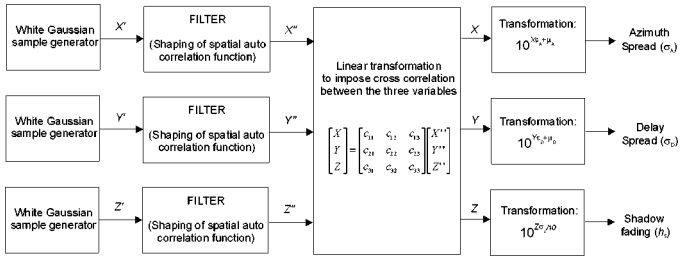

Fig. 11. Block diagram for joint simulation of the random variables describing the local AS, the local DS, and shadow fading component.

VII. Modeling Issues

Based on the results presented in Sections I–VI, it is possible to jointly simulate the random variables describing the local AS, the local DS, and the shadow fading component. These three random variables can be simulated according to the block diagram in Fig. 11. First, spatially white Gaussian noise samples are generated with zero mean and unit variance. These variables are subsequently filtered to obtain the correct spatial autocorrelation function. According to the results presented in Table III, it is reasonable to assume that all three variables have the same decorrelation distance. The cross correlation between the variables is imposed by using a simple linear transformation, where the coefficient of the transformation matrix (c_{mn}) can be computed from the cross-correlation coefficient presented in Table IV. Finally, the correlated Gaussian variables X, Y, and Z are transformed to the log-normal distributed variables describing the local AS, the local DS, and shadow fading according to (9), (10), and (13). The parameters required for these transformations are presented in Table II. Hence, Fig. 11 presents a simple low complexity method for simulation of the three random variables, based on the experimental results presented in this study.

VIII. Conclusion

The joint statistical behavior of the random variables describing the local AS, the local DS, and the shadow fading component has been characterized based on an analysis of measurement data. These measurement data were collected in outdoor macro cellular environments with the BS antenna elevated above rooftop level. All measurements were conducted with no line-of-sight (LOS) between the MS and the BS.

It is found that a log-normal distribution provides an accurate fit of the empirical pdf of both the local AS, the local DS, and the shadow fading component. The spatial autocorrelation function of the three random variables is found to follow an exponential decay for TU and BU environments. However, for SU environments, the spatial autocorrelation function of all three variables seems to be more accurately modeled with a double exponential decay. The decorrelation distance of the AS, DS, and shadow fading is observed to be nearly identical within each environment class. The fact that the pdf and the spatial autocorrelation function of the AS, DS, and shadow fading are identical indicates that the propagation mechanisms leading to these effects are strongly related. Especially for BU environments, where a strong positive cross correlation between AS and DS

is observed, while both the AS and the DS are negatively correlated with shadow fading. The same behavior is observed for the TU and SU environments, only with slightly lower cross-correlation coefficients.

The presented results provide sufficient information to jointly model the random behavior of the local AS, the local DS, and shadow fading component. This can help improve the reliability of e.g., the output of Monte Carlo network simulations of modern wideband mobile communication systems with BSs deploying advanced antenna array systems. Furthermore, the presented results can serve as useful *a priori* knowledge for planning and dimensioning purposes.

REFERENCES

[1] H. L. Bertoni, *Radio Propagation for Modern Wireless System*. Englewood Cliffs, NJ: Prentice-Hall, 2000.

[2] L. Correia, *Wireless Flexible Personalised Communications—Cost 259 Final Report*, New York: Wiley, 2001.

[3] J. G. Proakis, *Digital Communications*, 3rd ed. New York: McGraw-Hill, 1995.

[4] J. Winters, "Optimum combining in digital mobile radio with cochannel interference," *IEEE Trans. Veh. Technol.*, vol. VT-33, Aug. 1984.

[5] K. I. Pedersen, P. E. Mogensen, and B. H. Fleury, "Spatial channel characteristics in outdoor environments and their impact on BS antenna system performance," in *Proc. IEEE Vehicular Technology Conf. (VTC'98)*, Ottawa, Canada, May 1998, pp. 719–724.

[6] K. I. Pedersen and P. E. Mogensen, "Evaluation of vector-RAKE receivers using different antenna array configurations and combining schemes," *Int. J. Wireless Inform. Networks*, vol. 6, pp. 181–194, 1999.

[7] V. Veen and K. M. Buckley, "Beamforming: A versatile approach to spatial filtering," *IEEE Acoust., Speech Signal Processing (ASSP) Mag.*, pp. 4–24, Apr. 1988.

[8] J. Liberti and T. Rappaport, "A geometrically based model for line-of-sight multipath radio channels," in *Proc. IEEE Vehicular Technology Conf. (VTC 96)*, May 1996, pp. 844–848.

[9] M. Lu, T. Lo, and J. Litva, "A physical spatio-temporal model of multipath propagation channels," in *Proc. IEEE Vehicular Technology Conf. (VTC 97)*, May 1997, pp. 810–814.

[10] O. Nørklit and J. B. Andersen, "Diffuse channel model and experimental results for antenna arrays in mobile environments," *IEEE Trans. Antennas Propagat.*, vol. 96, pp. 834–840, June 1998.

[11] C. Cheon, H. L. Bertoni, and G. Liang, "Monte Carlo simulation of delay and angle spread in different building environments," presented at the Proc. IEEE Vehicular Technology Conf. (VTC'00), Boston, MA, Sept. 2000.

[12] K. I. Pedersen, P. E. Mogensen, and B. H. Fleury, "A stochastic model of the temporal and azimuthal dispersion seen at the base station in outdoor propagation environments," *IEEE Trans. Veh. Technol.*, vol. 49, pp. 437–447, Mar. 2000.

[13] U. Martin, "A directional radio channel model for densely built-up urban areas," in *Proc. European Personal Mobile Communications Conf. (EPMCC)*, Bonn, Germany, Oct. 1997, pp. 237–244.

[14] D. C. Cox, R. Murray, and A. Norris, "800 MHz attenuation measured in and around sub-urban houses," *AT&T Bell Lab. Tech. J.*, vol. 673, July–Aug. 1984.

[15] R. C. Bernhardt, "Macroscopic diversity in frequency reuse systems," *IEEE J. Select. Areas Commun.*, vol. 5, pp. 862–878, June 1987.

[16] M. Gudmundson, "Correlation model for shadow fading in mobile radio systems," *IEE Electron. Lett.*, vol. 27, pp. 2145–2126, Oct. 1992.

[17] A. Mawira, "Models for the spatial correlation functions of the log-normal component of the variability of VHF/UHF field strength in urban environment," in *Proc. Personal, Indoor and Mobile Radio Communications (PIMRC'92)*, 1992, pp. 436–440.

[18] A. Gehring, M. Steinbauer, I. Gaspard, and M. Grigat, "Empirical channel stationarity in urban environments," presented at the Proc. European Personal Mobile Communications Conf. (EPMCC), Vienna, Feb. 2001.

[19] T. B. Sørensen, "Correlation model for shadow fading in a small urban macro cell," presented at the Proc. Personal, Indoor and Mobile Radio Communications (PIMRC'98), Boston, 1998.

[20] "Algorithms and Antenna Array Recommendations," Public deliverable from European ACTS, TSUNAMI II Project, Deliverable code: AC020/AUC/A1.2/DR/P/005/bl, May 1997.

[21] F. Frederiksen, P. Mogensen, K. I. Pedersen, and P. Leth-Espensen, "A software testbed for performance evaluation of adaptive antennas in FH GSM and wideband-CDMA," in *Proc. 3rd ACTS Mobile Communication Summit*, vol. 2, Rhodes, Greece, June 1998, pp. 430–435.

[22] "Information Technologies and Sciences—Digital Land Mobile Radio Communications," Commission of the European Communities, COST 207, 1988.

[23] P. A. Bello, "Characterization of randomly time-variant linear channels," *IEEE Trans. Commun. Syst.*, vol. CS-11, pp. 360–393, Dec. 1963.

[24] J. A. Fessler and A. Hero, "Space-alternating generalized expectation-maximization algorithm," *IEEE Trans. Signal Processing*, vol. 42, pp. 2664–2677, Oct. 1994.

[25] B. H. Fleury, M. Tschudin, R. Heddergott, D. Dahlhaus, and K. I. Pedersen, "Channel parameter estimation in mobile radio environments using the SAGE algorithm," *IEEE J. Select. Areas Commun.*, vol. 17, pp. 434–450, Mar. 1999.

[26] K. I. Pedersen, B. H. Fleury, and P. E. Mogensen, "High resolution of electromagnetic waves in time-varying radio channels," in *Proc. Int. Symp. Personal Indoor and Mobile Radio Communications (PIMRC '97)*, Helsinki, Finland, Sept. 1997, pp. 650–654.

[27] K. I. Pedersen, P. Mogensen, B. H. Fleury, F. Frederiksen, and K. Olesen, "Analysis of time, azimuth and doppler dispersion in outdoor radio channels," in *Proc. ACTS Mobile Communication Summit '97*, Aalborg, Denmark, Oct. 1997, pp. 308–313.

[28] M. Hata, "Empirical formula for propagation loss in land mobile radio service," *IEEE Trans. Veh. Technol.*, vol. VT-29, pp. 317–325, 1980.

[29] L. J. Greenstein, V. Erceg, Y. S. Yeh, and M. V. Clark, "A new path-gain/delay-spread propagation model for digital cellular channels," *IEEE Trans. Veh. Technol.*, vol. 46, pp. 477–485, May 1997.

Albert Algans was born in Figueres (Catalonia), Spain, on July 14, 1977. He received the Enginyer de Telecomunicació (M.S.) degree from Universitat Politècnica de Catalunya, Barcelona, Spain, in September 2000. He is working on his Master Thesis at the Center for Personkommunikation (CPK), Aalborg University, Aalborg, Denmark.

In October 2000, he joined the Cellular Systems group in CPK working together with Nokia Networks Aalborg. He is currently working in fractal antennas for mobile communications in Fractus S.A., Spain.

Klaus Ingemann Pedersen (S'97–A'00) received the M.Sc.E.E. and Ph.D. degrees, in 1996 and 2000, respectively, from Aalborg University, Aalborg, Denmark.

He is currently with Nokia Networks in Aalborg, Denmark. His current research interests include radio resource managements for WCDMA systems, adaptive antenna array systems, and radio propagation.

Preben Elgaard Mogensen (S'88–M'89) received the M.Sc.E.E. and Ph.D. degrees, in 1988 and 1996, from Aalborg University, Denmark.

Since 1988, he has been with Aalborg University. He is currently holding a part time position of Research Professor and heading the Cellular Systems Research Group (CSYS) at the Center for Personkommunikation (CPK). Since 1995, he has worked part time with Nokia Networks and is now Manager of 3G Radio Systems Research team at NET/Aalborg, Denmark.